Applied Physics Letters ARTICLE scitation.org/journal/apl

# Similarity law and frequency scaling in low-pressure capacitive radio frequency plasmas

Cite as: Appl. Phys. Lett. **117**, 204101 (2020); doi: 10.1063/5.0029518
Submitted: 14 September 2020 · Accepted: 1 November 2020 ·
Published Online: 16 November 2020



Yangyang Fu,[1,2,a] Bocong Zheng,[3,a] De-Qi Wen,[1,2] Peng Zhang,[2] Qi Hua Fan,[2,3,4] and John P. Verboncoeur[1,2]

## AFFILIATIONS

[1]Department of Computational Mathematics, Science and Engineering, Michigan State University, East Lansing, Michigan 48824, USA
[2]Department of Electrical and Computer Engineering, Michigan State University, East Lansing, Michigan 48824, USA
[3]Fraunhofer Center for Coatings and Diamond Technologies, Michigan State University, East Lansing, Michigan 48824, USA
[4]Department of Chemical Engineering and Materials Science, Michigan State University, East Lansing, Michigan 48824, USA

[a]Authors to whom correspondence should be addressed: fuyangya@msu.edu and zhengboc@msu.edu

## ABSTRACT

We verify the similarity law (SL) and show a violation of frequency scaling (f-scaling) in low-pressure capacitive radio frequency (rf) plasmas via fully kinetic particle-in-cell simulations. The SL scaling relations for electron density and electron power absorption are first confirmed in similar rf discharges. Based on these results, with only the driving frequency varied, the f-scaling for electron density is also validated, showing almost the same trend as the SL scaling, across most of the frequency regime. However, violations of the f-scaling are observed at lower frequencies, which are found to be relevant to the electron heating mode transition from stochastic to Ohmic heating. Electron kinetic invariance is illustrated for the SL and f-scaling being valid, respectively, whereas the electron kinetic variation is observed when the f-scaling is violated.



Low-pressure radio frequency (rf) plasmas have attracted continuously growing attention due to their widespread applications.[1–5] In the past few decades, studies on the dynamical electron kinetics in rf plasmas have been extensively conducted to understand the fundamental discharge mechanisms, which provide the basis for the controllability and predictability of the discharge behaviors under different conditions.[6–9] Applied rf voltage $V_{rf}$, gas pressure $p$, gap distance $d$, and driving frequency $f$ are key parameters for tuning plasma properties, and various scaling laws are investigated with focus on the discharge dependence on the tuning parameter, revealing the effects of the gas pressure,[10–12] gap dimension,[13–16] and driving frequency[17–19] on the discharge behaviors. It has been generally recognized that for a given rf discharge chamber, tuning the driving frequency is an effective method to control the plasma density and the ion flux, which are essential for practical applications.[20,21] The frequency scaling (f-scaling) established the dependence of plasma density, sheath width, and power absorption on the rf driving frequency, which was verified by Surenda *et al.*[22] and Vahedi *et al.*[23] The f-scaling is also confirmed to be applicable for dual frequency and asymmetric capacitive rf discharges.[24,25] More recently, the effects of the driving frequency on the plasma density and the electron heating dynamics are still of broad interest.[26–28] However, understanding the validity of the scaling characteristics and their transition to possible violation regimes remains incomplete.

In this work, we verify the similarity law (SL) and show a violation of the f-scaling in low-pressure capacitive rf plasmas via particle-in-cell/Monte Carlo collision (PIC/MCC, 1d3v) simulations. First, the SL scaling relations for electron density and electron power absorption are confirmed under similar discharge conditions. Then, with only the driving frequency varied, we show that the f-scaling for electron density holds approximately the same scaling as the SL scaling, whereas violations of the f-scaling are observed at lower frequencies. Spatiotemporal and time-averaged distributions of the electron density and electron power absorption as well as the electron energy probability functions (EEPFs) under SL and f-scaling conditions are illustrated with comparative analysis, presenting explicit scaling features of the rf plasmas.

The SL method is usually used to established parameter scaling in similar discharges, which are usually generated in gaps of different dimensions but geometrically similar.[29,30] When similar discharges are

obtained, a physical parameter $G$ at the corresponding spatial and temporal points can be transformed between the original and scaled gaps by

$$G(x_1, t_1) = k^{\alpha[G]} G(x_k, t_k), \tag{1}$$

where $k = x_1/x_k = t_1/t_k$ is the scaling factor (this factor does not need to be an integer and can be less than one) and $\alpha[G]$ is the similarity factor for parameter $G$.[31,32] For similar rf discharges, discharge condition parameters scale as $k = p_k/p_1 = d_1/d_k = f_k/f_1$, keeping $f/p$ and $pd$ the same. Thus, from Eq. (1), we have $\alpha[x] = \alpha[t] = \alpha[d] = 1$ for the position, time, and gap distance, and $\alpha[p] = \alpha[f] = -1$ for gas pressure and driving frequency. Also, parameters having $\alpha[G] = 0$, such as $pd$ and $f/p$, are called similarity invariants. The most common similarity factors are $\alpha[n_e] = \alpha[\mathbf{J}_e] = -2$ for electron density $n_e$ and electron current density $\mathbf{J}_e$, $\alpha[\mathbf{E}] = -1$ for electric field $\mathbf{E}$, and $\alpha[\varepsilon_e] = \alpha[\mathbf{u}_e] = 0$ for electron energy $\varepsilon_e$ and electron velocity $\mathbf{u}_e$ in similar discharges.[29–32]

The simulations are performed with argon at 300 K, accounting for three electron-neutral collisions (elastic, excitation, and ionization scattering) and two ion-neutral collisions (isotropic and backward scattering).[33] The custom developed electrostatic PIC code, ASTRA, is used for all the simulations.[33,34] The rf plasmas are between two parallel-plate electrodes and geometrically symmetric, as shown in Fig. 1. In the SL scaling cases, the gas pressure, gap distance, and driving frequency are simultaneously changed, whereas in the f-scaling cases, the gas pressure and gap distance are fixed and only the driving frequency is tuned. The rf voltage waveform $V_{rf}(t) = 300 \cdot \sin(2\pi f t)[\mathrm{V}]$, where $f$ is the driving frequency with $T$ being the rf period, is connected to the powered electrode ($x = 0$), while the bottom electrode ($x = d$) is grounded. Secondary electron emission (SEE) induced by incident ions is considered and the SEE coefficient is 0.1; the electron reflection probability is zero for all the conditions. Electromagnetic effects (e.g., standing wave effect[1,2]) are not included, which are beyond the scope of this work.

Figure 2 shows the time-averaged electron density at the center of the gap in rf discharges at steady state and the scaling factor $k$ is from 1 to 10. In Fig. 2(a), $[p_k, d_k, f_k]$ are under the SL conditions and tuned through the scaling factor $k$ from the base case $[p_1, d_1, f_1] = [0.67\ \mathrm{Pa}, 10\ \mathrm{cm}, 13.56\ \mathrm{MHz}]$ with $k = 1$. The electron densities from PIC simulations with and without SEE both agree well with the

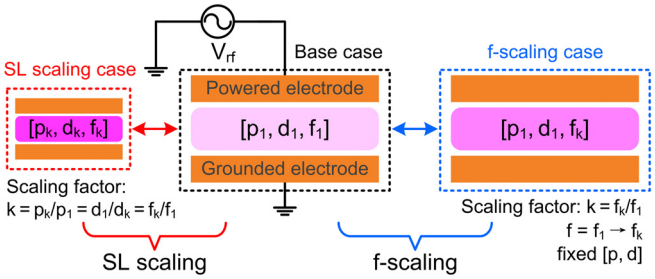


**FIG. 1.** Illustration of the rf discharge models. Under SL conditions, the gas pressure, gap distance, and driving frequency are simultaneously changed by a scaling factor $k = p_k/p_1 = d_1/d_k = f_k/f_1$, while under f-scaling conditions, the gas pressure and gap distance are fixed and the driving frequency is tuned by $k = f_k/f_1$.

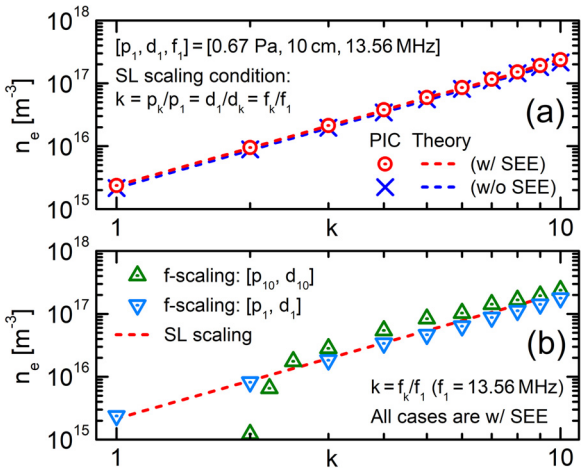


**FIG. 2.** (a) Verification of the SL scaling for the time-averaged electron density at the gap center with and without SEE; $[p_1, d_1, f_1] = [0.67\ \mathrm{Pa}, 10\ \mathrm{cm}, 13.56\ \mathrm{MHz}]$ is the base case with $k = 1$. (b) Illustration of the f-scaling for electron density with $[p_1, d_1] = [0.67\ \mathrm{Pa}, 10\ \mathrm{cm}]$, which holds approximately the same dependence on $k = f_k/f_1$ as the SL scaling does (dashed line), whereas violations of the f-scaling are observed for $[p_{10}, d_{10}] = [6.7\ \mathrm{Pa}, 1\ \mathrm{cm}]$ at lower frequencies.

theoretical SL prediction, showing a straight line with a slope of two in the log–log plot, which exactly confirms the electron density scaling, $k^{-2} n_e(k) = n_e(1)$, in similar discharges. The electron density proportional to $k^2$ can be understood through a fluid analysis from the electron continuity equation, which is expressed as

$$\frac{\partial n_e}{\partial t} + \frac{\partial (n_e \mathbf{u}_e)}{\partial x} = K_{iz} n_e N_g, \tag{2}$$

where $K_{iz}$ is the electron impact ionization rate coefficient and $N_g$ is the neutral gas number density ($N_g \propto p$). By dividing Eq. (2) with $k^3$, we have

$$\frac{\partial (k^{-2} n_e)}{\partial (kt)} + \frac{\partial (k^{-2} n_e \mathbf{u}_e)}{\partial (kx)} = K_{iz} (k^{-2} n_e)(k^{-1} N_g), \tag{3}$$

where $kt$, $kx$, $\mathbf{u}_e$, and $k^{-1}N_g$ are similarity invariants. From Eqs. (2) and (3), we can see that $n_e \propto k^2$ can be naturally satisfied when the discharges are similar, which have the same fundamental processes and can be described by the same equation. This scaling holds generally, not limited to rf discharges. However, it still assumes the same EEPF in the fluid model, and thus $K_{iz}$ is treated as a constant, not perturbed by the EEPF variation, in the compared systems. It is a simplified way to understand the fundamentals of the SL scaling, while a more exact analysis based on the scaling of the electron Boltzmann equation can be found in Ref. 32.

For the f-scaling shown in Fig. 2(b), we choose two cases ($k = 1$ and $k = 10$) from Fig. 2(a), and the driving frequency $f = f_k$ is swept one order of magnitude greater for $[p_1, d_1]$ and smaller for $[p_{10}, d_{10}]$, respectively. With $[p_1, d_1]$ fixed and $f_k$ increased, the electron density scaling to the frequency ratio $k = f_k/f_1$ closely follows the SL scaling under all the studied conditions, which verified the f-scaling for electron density $n_e(k) \propto k^2$ or equivalently $n_e(k) \propto f_k^2$.[23,25] For the case with $[p_{10}, d_{10}]$ fixed but $f_k$ decreased, the electron density first follows

the SL scaling but then departures from the f-scaling at lower frequencies with lower plasma densities. Interestingly, although the gas pressure and the gap distance are not tuned as the SL scaling does, the f-scaling holds the same scaling for electron density, expect for $[p_{10}, d_{10}]$ at lower frequencies. It is also worth noting that the electron densities with $[kp_1, d_1/k, f_k]$ are very close to those with $[p_1, d_1, f_k]$, which also implies that the rf plasma density will not be much altered when the f-scaling holds and $[p, d]$ are tuned dependently, keeping $pd$ = constant. Within the same degree of parameter variation, the plasma density is generally more sensitive to the driving frequency than to the gas pressure and gap distance.[7,35] However, a different selection of $[p, d]$ inevitably alters the range of the similarity invariant $f/p$ (or $fd$), which will result in a strong impact on the validity regime of the f-scaling.

To show more detailed features of the scaling, we present the spatiotemporal evolutions of the electron density under the SL and f-scaling conditions in Fig. 3. Under the SL conditions, as shown in Figs. 3(a)–3(c), electron density evolutions with $k = 10$, 5, and 2 are almost the same when the axes are normalized in both space and time. The maximum electron densities are $2.38 \times 10^{17}\ \mathrm{m}^{-3}$, $6.00 \times 10^{16}\ \mathrm{m}^{-3}$, and $9.45 \times 10^{15}\ \mathrm{m}^{-3}$ for $k = 10$, 5, and 2, respectively. One can also find that the scaled maximum electron density $k^{-2} n_e(k)$ is almost the same, which equals $2.38 \times 10^{15}\ \mathrm{m}^{-3}$ with the relative standard deviation of less than 1%. The results imply that the SL density scaling holds rigorously in both space and time domains. As for the f-scaling, electron density evolutions for $f_k = 67.8$ MHz, 33.9 MHz, and 27.12 MHz are shown in Figs. 3(d)–3(f) with $[p_{10}, d_{10}] = [6.7$ Pa, 1 cm] fixed. As the driving frequency decreases, the sheath width becomes much larger and, accordingly, the plasma bulk shrinks obviously. As shown in Fig. 2(b), the f-scaling holds for $f_k = 67.8$ MHz and 33.9 MHz but is violated for $f_k = 27.12$ MHz. However, the scaling of the spatiotemporal electron density does not hold as the SL scaling does since the discharge structures are different. In particular, in Fig. 3(f), the electron density profile becomes zigzag, without a stationary quasi-neutral bulk plasma, which could be accompanied by variations in the electron heating dynamics.

Figure 4 shows the electron power absorption calculated through $\mathbf{J}_e \cdot \mathbf{E}$, corresponding to the cases shown in Fig. 3. Similarly, it is observed that the electron heating evolutions are nearly rigorously maintained under the SL conditions, even for the oscillation features [see Figs. 4(a)–4(c)], which are caused by non-local beam electrons adjacent to the sheath edge.[28] The maximum and minimum electron heating rate divided by $k^3$ are almost the same. The results indicate that $k^{-3} \cdot \mathbf{J}_e \cdot \mathbf{E}$ is an invariant in similar discharges, which can also be consistently obtained from Eq. (1) since $\alpha[\mathbf{J}_e \cdot \mathbf{E}] = \alpha[\mathbf{J}_e] + \alpha[\mathbf{E}] = -3$. In Figs. 4(d)–4(e), as the driving frequency decreases, the electron heating rate decreases significantly, and the $\mathbf{J}_e \cdot \mathbf{E}$ magnitude is roughly proportional to $k^3$ (or equivalently $\propto f_k^3$), close to the SL scaling. However, in Fig. 4(f), the $\mathbf{J}_e \cdot \mathbf{E}$ magnitude significantly deviates from the SL scaling prediction, and also the $\mathbf{J}_e \cdot \mathbf{E}$ profile becomes very different from the typical rf discharges. It is not straightforward to confirm the scaling when the distribution and the magnitude are changing simultaneously. Therefore, we analyze the results by time averaging them in the following.

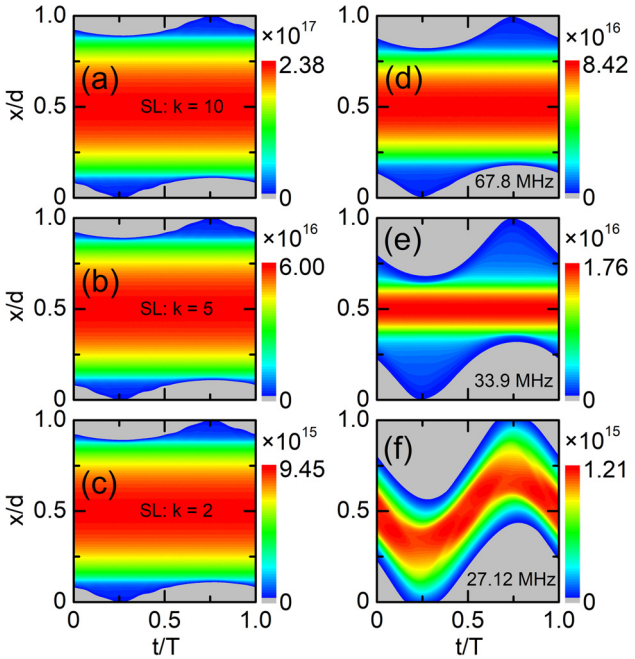


**FIG. 3.** Spatiotemporal electron density (unit in $\mathrm{m}^{-3}$) under SL and f-scaling conditions. Under the SL conditions (a)–(c), the scaling factors are (a) $k = 10$, (b) $k = 5$, and (c) $k = 2$, respectively; under the f-scaling conditions (d)–(f), $[p_{10}, d_{10}] = (6.7$ Pa, 1 cm) is fixed and the driving frequencies are (d) $f_k = 67.8$ MHz, (e) $f_k = 33.9$ MHz, and (f) $f_k = 27.12$ MHz, respectively.

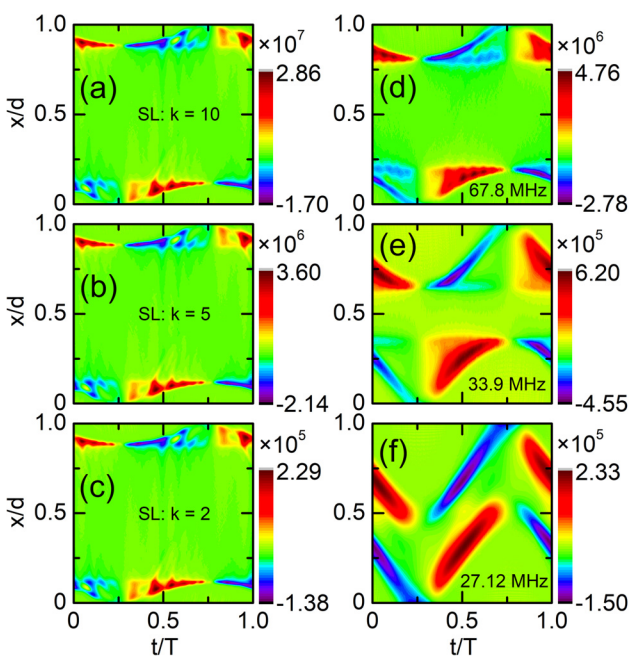


**FIG. 4.** Spatiotemporal electron power absorption (unit in $\mathrm{W} \cdot \mathrm{m}^{-3}$) under SL and f-scaling conditions. Under the SL conditions (a)–(c), the scaling factors are (a) $k = 10$, (b) $k = 5$, and (c) $k = 2$, respectively; under the f-scaling conditions (d)–(f), $[p_{10}, d_{10}] = [6.7$ Pa, 1 cm] is fixed and the driving frequencies are (d) $f_k = 67.8$ MHz, (e) $f_k = 33.9$ MHz, and (f) $f_k = 27.12$ MHz, respectively.

Considering that the electron power absorption mostly follows the SL scaling, in Fig. 5, we show the scaled time-averaged electron heating rate $k^{-3} \cdot \mathbf{J}_e \cdot \mathbf{E}$ for the analyzed cases. When the SL scaling is valid, as shown in Fig. 5(a), the scaled time-averaged heating rate is overlapping, which confirms the rigorously maintained SL scaling for electron heating, $P_e = \mathbf{J}_e \cdot \mathbf{E} \propto k^3$. It also implies that the SL scaling is expected at constant input power when the discharge volume is proportional to $k^{-3}$ in scaled devices for practical applications. Figure 5(b) shows the scaled electron heating rates under f-scaling conditions. While the magnitude of the scaled electron heating rate $k^{-3}P_{emax} = k^{-3} \cdot \mathbf{J}_e \cdot \mathbf{E}$ is quite close, three curves at different frequencies are distinguished by either the different sheath dimensions or the distribution profiles. When the f-scaling is still valid with $f_k = 67.8$ MHz ($k = 5$) and $f_k = 33.9$ MHz ($k = 2.5$), the averaged sheath widths are about 20% and 38% of the gap dimension, indicating the rf sheath scales inversely the frequency, i.e., $s \propto f_k^{-1}$ (or equivalently $s \propto k^{-1}$), which is consistent with the previous work by Lee *et al.*[25] For the cases with $f_k = 67.8$ MHz ($k = 5$) and $f_k = 33.9$ MHz ($k = 2.5$), the total electron power absorption per unit area can be approximately estimated through the area of the triangle [see Fig. 5(b)],

$$P_{abs} = 2\int_0^{d/2} \mathbf{J}_e \cdot \mathbf{E} dx \approx P_{emax} \cdot s \propto k^2, \quad (4)$$

where $P_{emax} \propto k^3$ is the maximum electron heating rate. The approximation in Eq. (4), though not rigorous, is a simplified way to express the power scaling when the f-scaling holds and the electron heating is mostly inside the time-average sheath region. Note that irregular distortions of the electron heating profile and potentially existing nonlinear sheath dynamics, especially under narrower sheath conditions,[10] may prohibit its validity; under such conditions, the integration should be exactly calculated. Since $k = f_k/f_1$ in our studied cases, the scaling of the total electron absorbed power [Eq. (4)] follows the scaling relation $P_{abs} \propto \omega^2 (\omega = 2\pi f)$ proposed by Lieberman *et al.* in Ref. 1.

Since the f-scaling is significantly violated for $k = 2$ (27.12 MHz), we decompose the scaled electron power absorption, as shown in Fig. 5(c), for more detailed examination. It can be observed that the dominant time-averaged heating is Ohmic (collisional) rather than stochastic (collisionless) heating and the non-Ohmic component is even negative. This heating mode is also recently observed by Vass *et al.* based on PIC simulations.[36] The cause for this is generally due to the attenuated component of the collisionless heating with the low plasma density and the sufficiently wide sheath [see Fig. 3(f)]. The electron power absorption due to the ambipolar field which usually has a maximum at the sheath edge is vanishing [see Fig. 4(f)], which leads to less deceleration of the energetic electrons and thus temporally more symmetric electron temperature within the rf period, resulting in the reduction of the collisionless heating on time average. The Ohmic heating, though small in magnitude, is positive across the gap and exhibits dominantly, while the collisionless components are mostly canceled out on time average (see Ref. 36 for more details). Although the observation of Vass *et al.* is at different pressures, this heating mode transition can also be tuned by the driving frequency, along with the violation of the f-scaling. Furthermore, from the point view of the SL scaling law, the fundamental processes and discharge mechanisms are maintained in similar discharges; therefore, when the combined discharge condition parameters $f/p$ and $pd$ are kept correspondingly the same, an observation of the dominant Ohmic heating on time average could be generally expected in the sustained rf plasmas. Based on those results, by further tuning the individual parameters, the heating mode transition can be identified in extended parameter regimes, and thereby, the violation of the f-scaling can be more effectively predicted.

The full space EEPFs under the SL and f-scaling conditions are shown in Fig. 6. When the SL scaling is valid, the EEPFs with different scaling factors are overlapping [see Fig. 6(a)], which confirms the

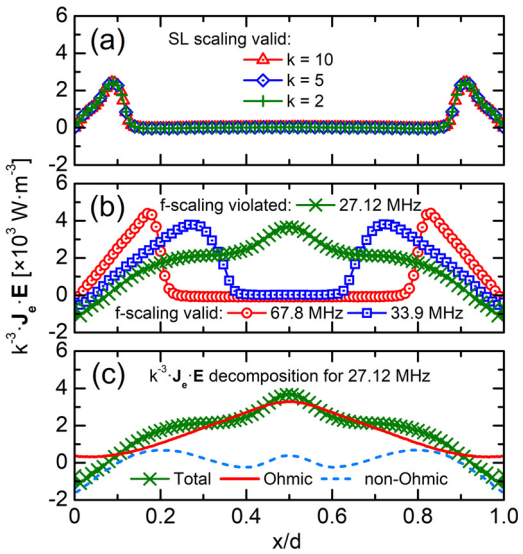


**FIG. 5.** Scaled time-averaged electron power absorption under different conditions. (a) SL scaling holds with all the curves overlapping. (b) f-scaling holds for $f_k = 67.8$ MHz ($k = 5$) and 33.9 MHz ($k = 2.5$) while is violated for $f_k = 27.12$ MHz ($k = 2$). (c) Decomposition of the scaled electron power absorption for $f_k = 27.12$ MHz, showing the dominant heating is Ohmic rather than stochastic.

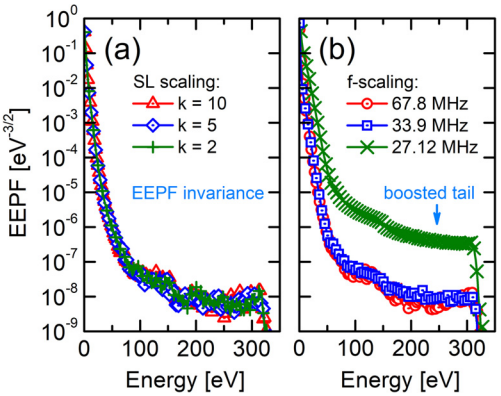


**FIG. 6.** (a) Under the SL conditions, EEPFs with $k = 10$, 5, and 2 are overlapping, which confirms the electron kinetic invariance in similar discharges. (b) Electron kinetic invariance is maintained when the f-scaling holds for $f_k = 67.8$ MHz and 33.9 MHz while is violated for $f_k = 27.12$ MHz with the EEPF having a more pronounced boosted tail.

electron kinetic invariance in similar discharges. Since the electron energy having $\alpha[\varepsilon_e] = 0$ is a similarity invariant, the same EEPFs guarantee the same mean electron temperature and correspondingly the same ionization rate coefficient [see Eqs. (2) and (3)] in compared systems, which maintained the similarity transformation for the electron density rigorously.[37] The high energy tails in the EEPF are generally due to secondary electrons, which can be accelerated to the highest energy corresponding to the maximum sheath voltage drop, $V_{rf}$ plus a plasma potential.[5,38]

For the f-scaling, as shown in Fig. 6(b), the EEPFs with $f_k = 67.8$ MHz and 33.9 MHz are also overlapping, which could largely exclude the parameter dependence on the electron temperature in determining the scaling laws. However, when the f-scaling is violated, for the case with $f_k = 27.12$ MHz, the EEPF is much different and has a more pronounced boosted tail in the high-energy region. As mentioned before, the plasma region at 27.12 MHz is narrower, and the transit time of the energetic electrons becomes less than the collision time; thus, these energetic electrons are less effectively confined, which are mostly ballistic and can be absorbed by the electrode without experiencing a collision or energy loss. Compared to other cases, the "collisionless" energetic beam-like electrons at 27.12 MHz largely preserve the kinetic energy during their lifetime, which boosts a more pronounced high energy tail in the EEPF. The EEPF variation can be also taken as an indicator to show the violation of the f-scaling.

Note that in this work, the SL scaling is only examined for the low-pressure *alpha* mode rf discharges, in which the secondary electron-induced heating and Ohmic heating are generally less important. Although here the rf plasmas are in symmetric gaps, the SL scaling is also expected to hold for asymmetrical rf discharges with the fundamental processes maintained. The SL scaling is rigorously maintained at low pressures, whereas at higher pressures, stepwise ionization becomes important, which may cause deviations from the confirmed scaling. For electronegative rf plasmas, since negative ions and ion-ion recombination are additionally considered and the discharge mode could be rather different (e.g., drift-ambipolar mode[39]), the applicability of the scaling laws should be further explored. As for the electrode surface processes, an inclusion of an energy-dependent SEE and non-zero electron reflection coefficient[40,41] would not compromise the SL scaling unless the electrodes are heated up and become strongly emissive (e.g., thermionic emission[42]).

In summary, we have verified the SL scaling and shown the violation of the f-scaling in capacitive rf discharges through kinetic simulations and comparative analysis. Under the SL conditions, the scaling relations for discharge parameters are rigorously maintained. On the basis of those results, we showed that with only the driving frequency varied, the f-scaling holds almost the same parameter dependence as the SL scaling. However, violations of the f-scaling are observed at low frequencies, which were identified to be accompanied by the electron heating mode transition, from the stochastic (collisionless) to Ohmic (collisional) dominant heating regime. The electron kinetic invariance is the most fundamental for achieving similar discharges, which is also observed when the f-scaling holds but is violated when the f-scaling breaks. This work explicitly illustrated the scaling validity and the violation mechanism relevant to the electron heating dynamics, which is essential for determining the effectiveness and predictability of scaling laws for rf plasma devices across a wide range of parameter regimes. Since the electron kinetics are largely modulated by the discharge conditions, we will also investigate the validity of the scaling laws with respect to the transitions in dominant electron heating mode (e.g., the *alpha* to *gamma* mode transition[2,19]), dc/rf hybrid or multi-frequency discharges, and potentially existing nonlinear electron dynamics (e.g., plasma series resonance[43]) in the future work.

This work was supported by the Air Force Office of Scientific Research Grant No. FA9550-18-1-0062, the Air Force Office of Scientific Research Grant No. FA9550-18-1-0061, the U.S. Department of Energy Office of Fusion Energy Science Grant No. DE-SC0001939, and the National Science Foundation Award Nos. 1917577 and 1724941.

## DATA AVAILABILITY

The data that support the findings of this study are available from the corresponding author upon reasonable request.

## REFERENCES

[1]M. A. Lieberman and A. J. Lichtenberg, *Principles of Plasma Discharges and Materials Processing* (John Wiley & Sons, New York, 2005).
[2]P. Chabert and N. Braithwaite, *Physics of Radio-Frequency Plasmas* (Cambridge University Press, Cambridge, 2011).
[3]S. Wilczek, J. Schulze, R. P. Brinkmann, Z. Donkó, J. Trieschmann, and T. Mussenbrock, J. Appl. Phys. **127**, 181101 (2020).
[4]J. Schulze, Z. Donkó, T. Lafleur, S. Wilczek, and R. P. Brinkmann, Plasma Sources Sci. Technol. **27**, 055010 (2018).
[5]L. Xu, L. Chen, M. Funk, A. Ranjan, M. Hummel, R. Bravenec, R. Sundararajan, D. J. Economou, and V. M. Donnelly, Appl. Phys. Lett. **93**, 261502 (2008).
[6]B. Bruneau, T. Gans, D. O'Connell, A. Greb, E. V. Johnson, and J.-P. Booth, Phys. Rev. Lett. **114**, 125002 (2015).
[7]Y.-X. Liu, Q.-Z. Zhang, W. Jiang, L.-J. Hou, X.-Z. Jiang, W.-Q. Lu, and Y.-N. Wang, Phys. Rev. Lett. **107**, 055002 (2011).
[8]G. Y. Park, S. J. You, F. Iza, and J. K. Lee, Phys. Rev. Lett. **98**, 085003 (2007).
[9]T. Mussenbrock, R. P. Brinkmann, M. A. Lieberman, A. J. Lichtenberg, and E. Kawamura, Phys. Rev. Lett. **101**, 085004 (2008).
[10]T. H. Chung, H. S. Yoon, and J. K. Lee, J. Appl. Phys. **78**, 6441 (1995).
[11]Y. Fu, J. Krek, D. Wen, P. Zhang, and J. P. Verboncoeur, Plasma Sources Sci. Technol. **28**, 095012 (2019).
[12]Y. Fu, P. Zhang, and J. P. Verboncoeur, Appl. Phys. Lett. **113**, 054102 (2018).
[13]K. Bera, S. Rauf, K. Ramaswamy, and K. Collins, J. Vac. Sci. Technol., A **27**, 706 (2009).
[14]A. Venkattraman and A. A. Alexeenko, Phys. Plasmas **19**, 123515 (2012).
[15]A. M. Loveless and A. L. Garner, Appl. Phys. Lett. **108**, 234103 (2016).
[16]Y. Fu, P. Zhang, J. P. Verboncoeur, and X. Wang, Plasma Res. Express **2**, 013001 (2020).
[17]Y. T. Zhang, Q. Q. Li, J. Lou, and Q. M. Li, Appl. Phys. Lett. **97**, 141504 (2010).
[18]J. L. Walsh, Y. T. Zhang, F. Iza, and M. G. Kong, Appl. Phys. Lett. **93**, 221505 (2008).
[19]M. U. Lee, J. Lee, J. K. Lee, and G. S. Yun, Plasma Sources Sci. Technol. **26**, 034003 (2017).
[20]Z. Donkó, J. Schulze, P. Hartmann, I. Korolov, U. Czarnetzki, and E. Schüngel, Appl. Phys. Lett. **97**, 081501 (2010).
[21]S. Sharma, A. Sen, N. Sirse, M. M. Turner, and A. R. Ellingboe, Phys. Plasmas **25**, 080705 (2018).
[22]M. Surendra and D. B. Graves, Appl. Phys. Lett. **59**, 2091 (1991).
[23]V. Vahedi, C. K. Birdsall, M. A. Lieberman, G. DiPeso, and T. D. Rognlien, Phys. Fluids B **5**, 2719 (1993).
[24]E. Semmler, P. Awakowicz, and A. Von Keudell, Plasma Sources Sci. Technol. **16**, 839 (2007).
[25]J. K. Lee, O. V. Manuilenko, N. Y. Babaeva, H. C. Kim, and J. W. Shon, Plasma Sources Sci. Technol. **14**, 89 (2005).

[26]S. Sharma, N. Sirse, M. M. Turner, and A. R. Ellingboe, Phys. Plasmas **25**, 063501 (2018).
[27]S. Sharma, N. Sirse, P. Kaw, M. M. Turner, and A. R. Ellingboe, Phys. Plasmas **23**, 110701 (2016).
[28]S. Wilczek, J. Trieschmann, J. Schulze, E. Schuengel, R. P. Brinkmann, A. Derzsi, I. Korolov, Z. Donkó, and T. Mussenbrock, Plasma Sources Sci. Technol. **24**, 024002 (2015).
[29]Y. Fu, G. M. Parsey, J. P. Verboncoeur, and A. J. Christlieb, Phys. Plasmas **24**, 113518 (2017).
[30]Y. Fu, P. Zhang, J. Krek, and J. P. Verboncoeur, Appl. Phys. Lett. **114**, 014102 (2019).
[31]A. A. Rukhadze, N. N. Sobolev, and V. V. Sokovikov, Sov. Phys. Usp. **34**, 827 (1991).
[32]Y. Fu, B. Zheng, P. Zhang, Q. H. Fan, J. P. Verboncoeur, and X. Wang, Phys. Plasmas **27**, 113501 (2020).
[33]B. Zheng, K. Wang, T. Grotjohn, T. Schuelke, and Q. H. Fan, Plasma Sources Sci. Technol. **28**, 09LT03 (2019).
[34]B. Zheng, Y. Fu, D.-Q. Wen, K. Wang, T. Schuelke, and Q. H. Fan, J. Phys. D: Appl. Phys. **53**, 435201 (2020).
[35]V. Godyak, R. Piejak, and B. Alexandrovich, J. Appl. Phys. **73**, 3657 (1993).
[36]M. Vass, S. Wilczek, T. Lafleur, R. P. Brinkmann, Z. Donkó, and J. Schulze, Plasma Sources Sci. Technol. **29**, 085014 (2020).
[37]Y. Fu and J. P. Verboncoeur, IEEE Trans. Plasma Sci. **47**, 1994 (2019).
[38]Y. Fu, B. Zheng, D.-Q. Wen, P. Zhang, Q. H. Fan, and J. P. Verboncoeur, Plasma Sources Sci. Technol. **29**, 09LT01 (2020).
[39]J. Schulze, A. Derzsi, K. Dittmann, T. Hemke, J. Meichsner, and Z. Donkó, Phys. Rev. Lett. **107**, 275001 (2011).
[40]M. Daksha, A. Derzsi, S. Wilczek, J. Trieschmann, T. Mussenbrock, P. Awakowicz, Z. Donkó, and J. Schulze, Plasma Sources Sci. Technol. **26**, 085006 (2017).
[41]B. Horváth, J. Schulze, Z. Donkó, and A. Derzsi, J. Phys. D: Appl. Phys. **51**, 355204 (2018).
[42]M. Campanell and M. Umansky, Phys. Rev. Lett. **116**, 085003 (2016).
[43]S. Wilczek, J. Trieschmann, D. Eremin, R. P. Brinkmann, J. Schulze, E. Schuengel, A. Derzsi, I. Korolov, P. Hartmann, Z. Donkó, and T. Mussenbrock, Phys. Plasmas **23**, 063514 (2016).